The Electron Density Distribution in Be Metal Obtained from Synchrotron-Radiation Powder Data by the Maximum-Entropy Method *

Masaki Takata, Yoshiki Kubota, and Makoto Sakata

Department of Applied Physics, Nagoya University, Nagoya, 464-01, Japan

Z. Naturforsch. **48a,** 75–80 (1993); received December 28, 1991

The nature of the bonding in Be metal was studied by investigating the MEM map, which is the electron density distribution obtained by the Maximum-Entropy Method. In order to avoid extinction effects, 19 Bragg reflections were measured by a new powder-diffraction experiment that utilizes Synchrotron Radiation as an incident X-ray and an Imaging Plate as detector. The experiment was carried out at the Photon Factory BL6A2. In spite of the limited number of reflections used in the MEM analysis, the electron density distribution of Be was obtained accurately and reliably. The structure factors for unmeasured reflections were calculated and compared with the values observed by Larsen and Hansen [Acta Cryst. **B 40,** 169 (1984)]. The agreement is very good. Furthermore, the MEM map revealed that Be metal forms an electronic layer in the shape of a honeycomb that is parallel to the basal plane.

Key words: Maximum entropy method; Be metal; Electron density distribution; X-ray powder diffraction; HCP structure.

Introduction

The electron density distribution in Be metal has been studied by several authors in the past two decades in order to reveal the features of bonding charge. Brown [1] measured X-ray structure factors for the 27 Bragg reflections with $(\sin\theta/\lambda) < 0.88$ Å^{-1} on an absolute scale. She proposed a model involving a 2p-like tight-binding wave function to account for the discrepancies of the observed and calculated structure factors. Stewart [2] reanalyzed her data with multipole refinements and reported that the valence maps showed bonding charge density between Be atoms along the *c*-axis through the tetrahedral vacancy. Yang and Coppens [3] studied the bonding in Be metal by recalculating the valence electron density and deformation density maps from Brown's data. Larsen and Hansen [4] measured X-ray structure factors of Be with even higher resolution, viz. $(\sin\theta/\lambda) \leqq 1.41$ Å^{-1}. Hansen et al. [5] carried out a γ-ray diffraction experiment. In these studies, the charge density distributions of Be were analyzed by Fourier methods and compared with results of theoretical studies [6, 7].

Recently it was found [8] that the Maximum-Entropy Method (MEM) is very powerful for examination of the electronic structure of crystalline solids. The MEM analysis yields an improvement of resolution and enables one to derive an electron density distribution that is consistent with the observed structure-factor data and least biased with respect to unobserved structure factors without introducing any structural model. Thus it can be said that the MEM minimizes termination effects of Fourier summation. By the MEM, Sakata and Sato [8] have revealed the features of the covalent bonding of Si using data obtained by the X-ray Pendellösung method [9]. The fundamental features of the resultant electron density were consistent with the valence electron density [10] obtained by a pseudopotential calculation with core-orthogonalization terms.

For the MEM analysis it is very important to collect reliable data since a structural model is not used in this method. In terms of the study of electron density distributions by X-ray diffraction methods, it is generally known that the deformation of the electron density in crystalline solids, which shows a widely spread distribution in real space, contributes mostly to the forward scattering. Therefore, reliability of observed data is required especially in the low-angle region. By X-ray single crystal diffraction, lower-angle data tend to be affected by extinction and must be

* Presented at the Sagamore X Conference on Charge, Spin, and Momentum Densities, Konstanz, Fed. Rep. of Germany, September 1–7, 1991.

Reprint requests to Dr. Masaki Takata, Department of Applied Physics, Nagoya University, Nagoya, 464-01, Japan.

0932-0784 / 93 / 0100-0075 $ 01.30/0. – Please order a reprint rather than making your own copy.

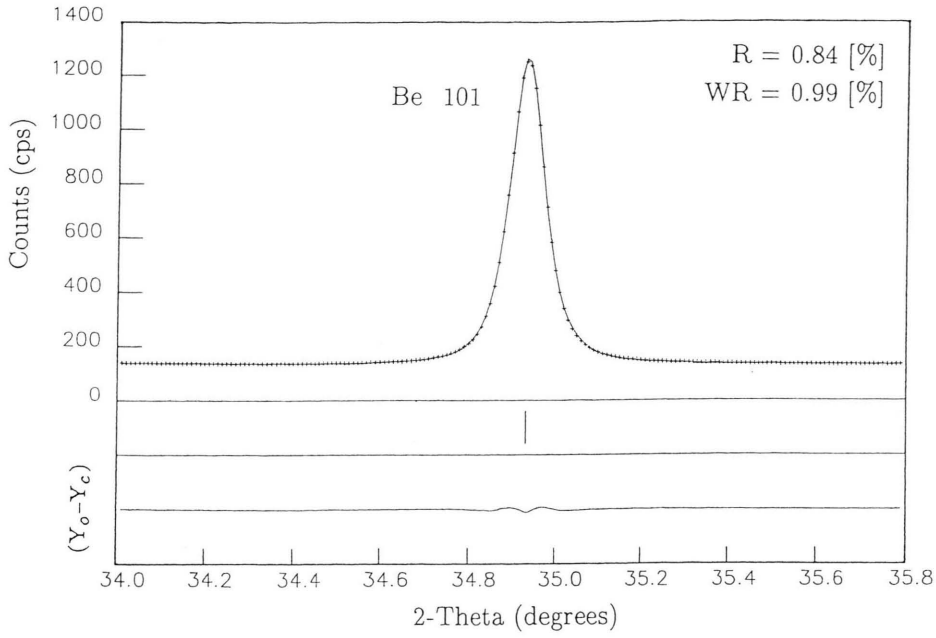

Fig. 1. Profile fitting for the Be [101]-reflection. Experimental points are plotted with +. The solid line shows calculated values. The differences of the observed and calculated intensities are shown below as $Y_o - Y_c$.

corrected by a method that depends on the structure model employed. Powder diffractometry makes it possible to collect reliable data with less risk of artificial bias such as extinction. Sakata et al. [11, 12] showed that reliable electron density data could be obtained from X-ray powder data by the MEM. Powder diffractometry has not been used to investigate the electron density distribution in Be metal. The purpose of the present work is to study the features of bonding in Be metal by using the newly developed method.

Experiment

In order to obtain a reliable charge density in Be, our main effort was to collect precise powder-diffraction data. For this purpose, a new powder-diffraction method [13, 14], that is composed of a combination of Synchrotron Radiation (SR) and an Imaging Plate (IP), was adopted. The powder sample is mounted in a thin-wall capillary of 0.3 mm diameter. This experimental technique is suitable for materials composed of only light elements because the experiment is carried out in transmission geometry.

The X-ray powder data for Be were collected by the large Debye-Scherrer camera (radius 572 mm) at the Photon Factory BL6A2. The resolution of the angle 2θ was 0.01°. The wavelength of the incident X-rays was 1.04 Å. In order to obtain an X-ray powder pattern with good counting statistics, the diffracted intensities were accumulated on an IP for 5 hours, which is a rather long exposure time for IP experiments. Other experimental arrangements are described in detail in [13, 14]. In the present experiment a powder pattern with 19 low-angle Bragg reflections was obtained.

Powder Data Analysis

The integrated intensities for each Bragg reflection were measured by the profile fitting technique. The profile analysis was carried out by the computer program PROFIT [15]. The split Pearson-VII function was employed as a profile function in the present analysis. As an example, the result of profile fitting for the strongest reflection, which is [101], is shown in Figure 1. The R-value of profile fitting was 0.99%. It is understood that the profile function gave an excellent fit. By this analysis, the integrated intensity of [101] is determined with an error of 0.3%, if the error can be estimated by the agreement of profile fitting. Finally, the integrated intensities were determined for the 19

individual reflections with errors less than 5%. When the integrated intensities were converted to structure factors, the relative errors for the structure factors became less than 1.4%.

The MEM Map of Be

The details of the procedure to obtain MEM density distributions from powder data are given in [8, 10]. The present theory of MEM is based on Collins's formalism [16]. For Be, the number of the pixels used is $60 \times 60 \times 60$.

In order to present the results of the MEM analysis, the MEM density map, which is the electron density distribution map obtained by the MEM, will be shown. In Fig. 2, the MEM density map of the Be (110)-plane is shown. Fig. 2 (a) and (b) show higher and lower-electron-density regions, respectively. There is no negative-electron-density region in the MEM map. In Fig. 2 (a), only atomic sites appear as sharp maxima of the electron density with a peak value of 50.1 e/Å^3. These electrons correspond to core electrons of the Be atoms, which are usually not shown by the conventional deformation map. In Fig. 2 (b), apart from electrons around atomic sites, small peaks of the electron density can be seen in the bipyramidal space around the tetrahedral holes, which are indicated by T. On the other hand, compared with the tetrahedral holes, the depletion of electrons can be observed in the channel formed by adjoining octahedral holes along the *c*-axis. Such depiction of the electron density is consistent with the deformation and valence maps in other works [3–5]. It should be noted that the present results are obtained in the form of an electron density purely from experimental data and free from any structural model. These characteristic features imply that the bonding nature of Be cannot be described by a simple metallic bonding of the nearly-free electron model. The bonding of Be has been interpreted as the deformation due to the hybridization of the s- and p-orbitals in the Be crystal [3, 4].

The electron density at the small peak close to the tetrahedral hole in the MEM map is 0.37 e/Å^3. The experimental valence map of Larsen et al. [4] and the LCAO theoretical valence map [7] gave a slightly smaller value, viz. 0.3 e/Å^3. The difference may not be significant because the MEM map gives total electron densities whereas other works deal with valence electrons only. Therefore it was concluded that a reliable electron density could be obtained by the MEM without introducing any structural model from X-ray powder data. The present results could provide instructive information for theoretical studies, although more elaborate examination is necessary for details of the features in the MEM map.

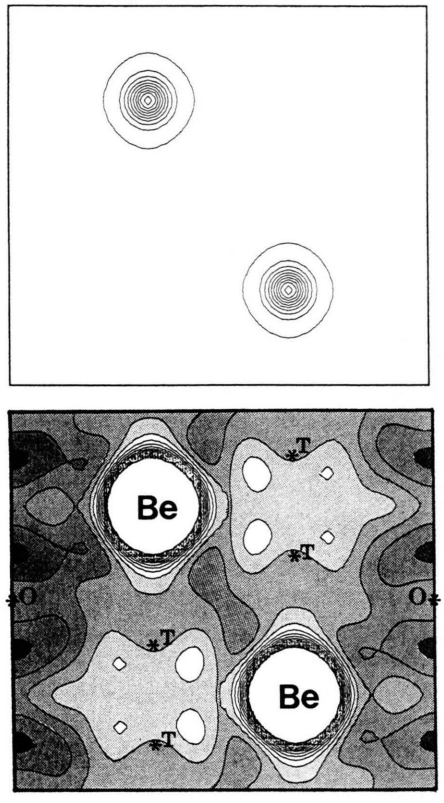

Fig. 2. MEM maps of (110) for Be. (a) The higher-electron-density region from 1.0 to 50.0 e/Å^3 with 0.5 e/Å^3 step width. (b) The lower-electron-density region from 0.0 to 1.0 e/Å^3 with 0.05 e/Å^3 step width. The lower-density regions are shaded according to the density, the darker the lower. The tetrahedral holes and the octahedral holes are marked by T and O, respectively.

The Resolution of the MEM Map

The MEM is basically a method of a statistical deduction. It is, therefore, possible to calculate the deduced structure factors from an MEM density map for unmeasured Bragg reflections. In order to demonstrate that, the calculated structure factors from the MEM map are shown in Fig. 3 together with the observed values of Larsen and Hansen [4]. The structure

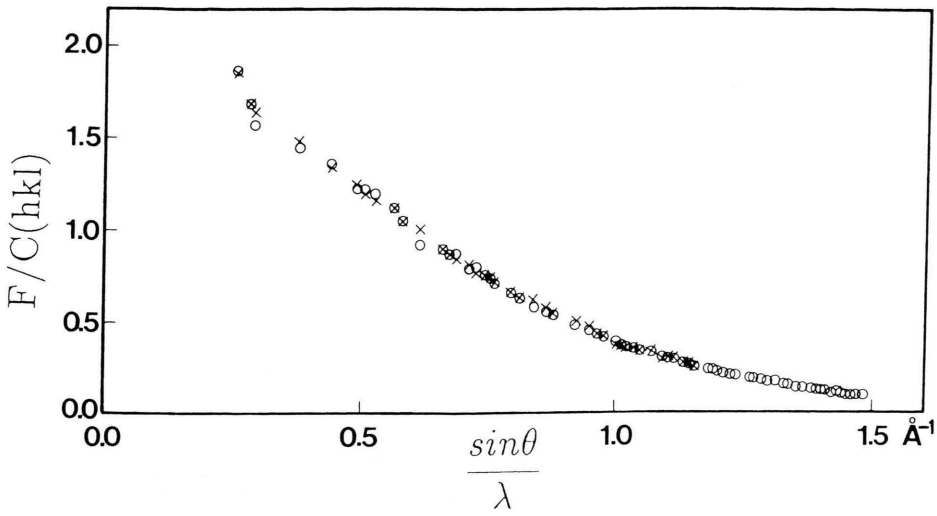

Fig. 3. The plots of $F(hkl)/C(hkl)$ vs. $\sin\theta/\lambda$ with calculated values (o) and Larsen and Hansen's data (×). $C(hkl)$ is the phase factor.

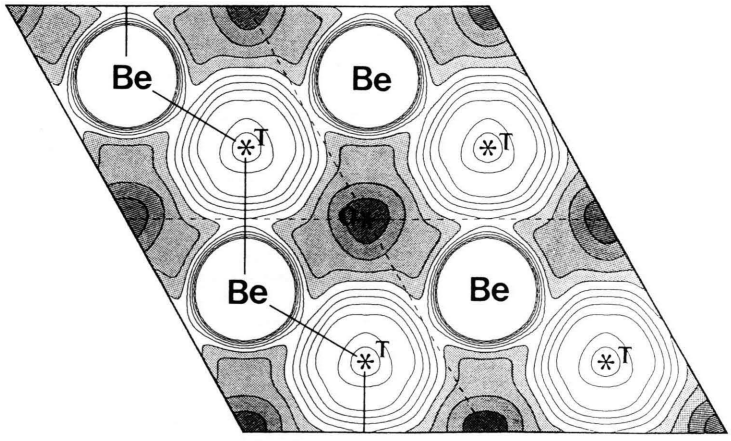

Fig. 4. The projected MEM map of Be basal plane. This is a projected map over one stacking layer. The contour lines are plotted from 0.0 to 10.0 e/Å^3 with 0.5 e/Å^3 step width.

factors obtained in the present study and other published structure factors are also listed in Table 1. For unmeasured reflections, the calculated values show very good agreement with the experimental values. In this study, only 19 lowest-angle structure factors were used for the MEM analysis. The present results, however, were not affected severely by the termination effects of the Fourier summation. The demonstration shown in Fig. 3 explains the reason well.

The Electronic Layer Structure of Be

In the MEM map, the electron localized in the space around a tetrahedral hole can be observed simultaneously with the electron density of the atomic sites, as shown in Figure 2. This gives a big advantage in examining the nature of chemical bonding in the crystal. In order to observe the distribution of the localized electron around the tetrahedral holes as well as that of the atomic sites in the basal plane, the MEM map projected for one stacking layer is shown in Figure 4. In this figure, the contour lines are shown only for the lower-electron-density region. The localization of the electron density is clearly shown in the space around a tetrahedral hole, whereas the electron density is shallow in the space around an octahedral hole. It is also seen that the localized electrons around the tetrahedral hole form a multi-center bond and are connect-

Table 1. MEM, experimental and theoretical structure factors of Be. F (MEM) are the structure factors calculated from the MEM map.

			Present study		Experimental			Theory (LCAO)
h	k	l	Powder data	F (MEM)	Larsen Ref. [4]	Brown Ref. [1]	Hansen Ref. [5]	Dovesi Ref. [7]
1	0	0	1.86 (2)	1.872	1.85 (2)	1.715 (6)	1.82 (1)	1.8923
0	0	2	3.13 (3)	3.380	3.37 (3)	2.98 (2)	3.34 (3)	3.3984
1	0	1	2.81 (3)	2.720	2.84 (3)	2.606 (6)	2.82 (3)	2.7983
1	0	2	1.40 (1)	1.450	1.48 (1)	1.403 (4)	1.488 (8)	1.4345
1	1	0	2.73 (3)	2.729	2.69 (2)	2.502 (9)	2.65 (1)	2.6318
1	0	3	2.07 (2)	2.130	2.17 (2)	2.019 (8)	2.17 (1)	2.1319
2	0	0	1.23 (2)	1.233	1.20 (1)	1.129 (4)	1.207 (8)	1.1824
1	1	2	2.36 (2)	2.356	2.35 (2)	2.191 (8)	2.36 (1)	2.3304
2	0	1	2.07 (2)	2.073	2.02 (2)	1.889 (7)	2.02 (1)	1.9978
0	0	4	2.10 (3)	2.257	2.23 (2)	2.04 (1)	2.19 (1)	2.2015
2	0	2	1.03 (1)	1.041	1.05 (1)	0.997 (3)	1.045 (7)	1.0496
1	0	4	–	0.921	1.00 (1)	0.943 (3)	0.330 (7)	0.9896
2	0	3	1.52 (2)	1.547	1.561 (4)	1.483 (4)	1.559 (9)	1.5568
2	1	0	0.88 (2)	0.888	0.869 (2)	0.818 (3)	0.852 (8)	0.8683
2	1	1	1.51 (2)	1.513	1.459 (3)	1.367 (4)	1.444 (7)	1.4590
1	1	4	1.54 (2)	1.586	1.617 (3)	1.523 (8)	1.584 (9)	1.6120
2	1	2	0.79 (1)	0.802	0.768 (1)	0.710 (5)	0.756 (7)	0.7703
1	0	5	1.25 (2)	1.301	1.316 (3)	1.232 (6)	1.283 (8)	1.3070
2	0	4	0.70 (1)	0.714	0.732 (2)	0.679 (6)	0.722 (7)	0.7297
3	0	0	1.44 (2)	1.444	1.418 (3)	1.306 (5)	1.399 (9)	1.4208
2	1	3		1.130	1.150 (3)	1.080 (5)	1.155 (7)	1.1540
3	0	2		1.267	1.260 (3)	1.165 (4)	1.257 (8)	1.2671
0	0	6		1.162	1.220 (3)	1.079 (9)	1.20 (2)	1.2147
2	0	5		0.954	0.984 (2)	0.893 (1)	0.946 (7)	0.9803
2	1	4		0.545	0.545 (2)	0.514 (6)	0.52 (1)	0.5482
1	0	6		0.529	0.555 (1)	0.507 (6)	–	0.5534
2	2	0		1.100	1.063 (2)	0.998 (5)	1.042 (8)	1.0682
3	1	0		0.496	0.488 (1)		0.48 (1)	
2	2	2		0.985	0.955 (2)		0.943 (7)	
3	1	1		0.860	0.817 (2)		0.814 (6)	
3	0	4		0.911	0.908 (2)		0.925 (7)	
1	1	6		0.896	0.926 (2)		0.933 (7)	
3	1	2		0.443	0.439 (1)		0.42 (2)	
2	1	5		0.733	0.746 (2)		0.745 (8)	
2	0	6		0.410	0.421 (1)		–	
3	1	3		0.687	0.662 (1)		0.644 (8)	
1	0	7		0.665	0.685 (2)		–	
4	0	0		0.408	0.366 (2)		–	
4	0	1		0.661	0.628 (2)		–	
2	2	4		0.713	0.704 (2)		0.690 (9)	
4	0	2		0.364	0.336 (1)		–	
3	1	4		0.325	0.324 (1)		–	
2	1	6		0.324	0.329 (1)		–	
4	0	3		0.534	0.516 (1)		–	
2	0	7		0.518	0.528 (1)		–	
3	2	0		0.316	0.288 (1)		–	
3	2	1		0.524	0.485 (1)		–	
0	0	8		0.582	0.594 (3)		0.59 (2)	
3	0	6		0.548	0.553 (1)		–	
3	2	2		0.283	0.261 (1)		–	
1	0	8		0.264	0.275 (1)		–	
3	1	5		0.456	0.452 (1)		–	
4	0	4		0.266	0.249 (2)		–	
4	1	0		0.534	0.491 (1)		0.50 (1)	
3	2	3		0.426	0.405 (1)			
2	1	7		0.406	0.419 (1)			
4	1	2		0.481	0.447 (1)			
1	1	8		0.455	0.466 (2)			
2	2	6		0.434				
2	0	8		0.209				
	⋮			⋮				
	⋮			⋮				

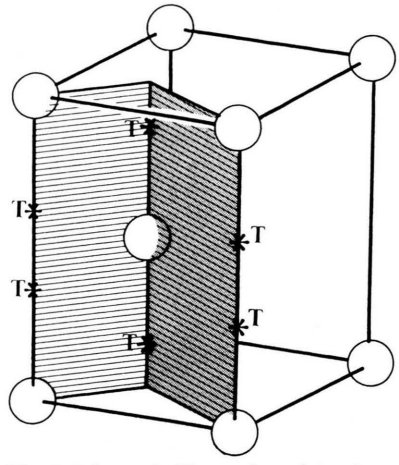

Fig. 5. Schematic illustration of the zigzag plane composed of {110}-planes indicated by solid lines in Figure 4.

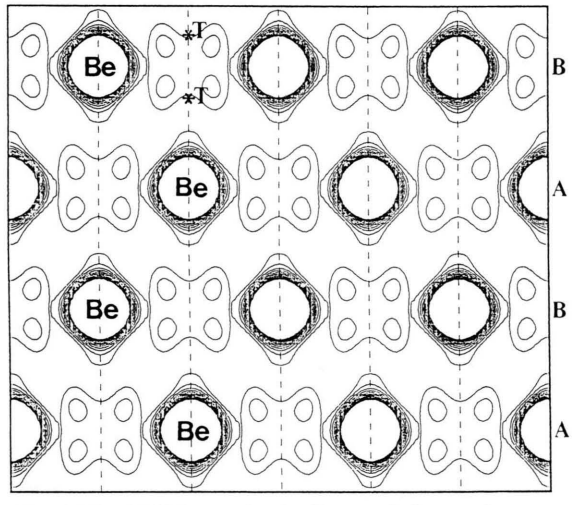

Fig. 6. The MEM map in the flattened zigzag plane represented in Figure 5. The contour lines are plotted from 0.3 to 1.0 e/Å^3 with 0.05 e/Å^3 step width.

ing atoms forming a honeycomb network in one stacking layer.

In order to examine the configuration of such a network of localized electrons further, a new kind of illustration of the electron density distribution is tried, viz. the MEM density map in the zigzag plane composed of crystallographically equivalent {110}-planes along the network that is indicated by the solid line in Figure 4. This zigzag plane is represented schematically in Figure 5. The MEM map of the zigzag plane is shown for four stacking layers in Fig. 6 to demon-

strate the connectivity well. The figure reveals that the localized electrons in the space around a tetrahedral hole are connecting the atoms within the (001) atomic plane, and there is no overlap of electrons between the planes. Consequently, it can be said that the Be atoms form an electronic layer structure in the hcp crystal.

The plastic deformation modes by slip [17] in the hexagonal close-packed structure have been investigated early in this century by many authors. For Be crystals, the slip occurring along the (001) basal plane is reported as the primary slip mode. This seems to have a close relationship with the feature of the electronic layer structure in Be obtained in this study if it is assumed that the localized electron density in the tetrahedral hole acts as a bonding electron. This suggests that the MEM map could provide an atomistic understanding of the elastic properties. Further investigation of the MEM maps of other hcp metals such as Zn, Mg, etc. is necessary to explain the relationship between the configuration of the localized electrons and the slip deformation of an hcp metal.

In conclusion, by the MEM map obtained from our powder data, new aspects were revealed for the electron density distribution in Be metal.

The authors thank Prof. N. Sakabe and Drs. A. Nakagawa and N. Watanabe of Photon Factory for their kind help and suggestions in data collection. We thank Mr. S. Kumazawa for improvement of the computer program of the MEM. This work was supported by Grant-in-Aid for Research from the Ministry of Education, Science and Culture and has been performed under the approval of the Photon Factory Program Advisory Committee (Proposal No. 91-244).

[1] P. J. Brown, Philos. Mag. **26,** 1377 (1972).
[2] R. F. Stewart, Acta Cryst. **A 33,** 33 (1977).
[3] Y. W. Yang and P. Coppens, Acta Cryst. **A 34,** 61 (1978).
[4] F. K. Larsen and N. K. Hansen, Acta Cryst. **B 40,** 169 (1984).
[5] N. K. Hansen, J. R. Schneider, W. B. Yelon, and W. H. Pearson, Acta Cryst. **A 43,** 763 (1987).
[6] S. T. Inoue and J. Yamashita, J. Phys. Soc. Japan **35,** 677 (1973).
[7] R. Dovesi, C. Pisani, F. Ricca, and C. Roetti, Phys. Rev. B **25,** 3731 (1982).
[8] M. Sakata and M. Sato, Acta Cryst. **A 46,** 263 (1990).
[9] T. Saka and N. Kato, Acta Cryst. **A 42,** 469 (1986).
[10] H. Nara, Private communication 1991.
[11] M. Sakata, R. Mori, S. Kumazawa, M. Takata, and H. Toraya, J. Appl. Cryst. **23,** 526 (1990).
[12] M. Sakata, T. Uno, M. Takata, and R. Mori, Acta Cryst. **B 48,** 591 (1992).
[13] M. Takata, M. Yamada, and M. Sakata, Photon Factory Activity Report, **8,** 103 (1990).
[14] M. Takata, M. Yamada, Y. Kubota, and M. Sakata, Advances in X-Ray Analysis **35,** 85 (1992).
[15] H. Toraya, J. Appl. Cryst. **19,** 440 (1986).
[16] D. M. Collins, Nature London **298,** 49 (1982).
[17] M. H. Yoo and C. T. Wei, J. Appl. Physics **38,** 4317 (1967).